


Article

Modeling of Quantitative Characterization Parameters and Identification of Fluid Properties in Tight Sandstone Reservoirs of the Ordos Basin

Bo Xu ^{1,2} , Zhenhua Wang ³, Ting Song ⁴, Shuxia Zhang ³, Jiao Peng ^{1,2}, Tong Wang ^{1,2,*} and Yatong Chen ^{1,2}

¹ School of Petroleum Engineering, Xi'an Shiyou University, Xi'an 710065, China; bxu@xsyu.edu.cn (B.X.); jp@xsyu.edu.cn (J.P.); c12370904@126.com (Y.C.)

² Key Laboratory of Special Stimulation Technology for Oil and Gas Fields in Shaanxi Province, Xi'an 710065, China

³ Research Institute of Shannxi Yanchang Petroleum (Group) Co., Ltd., Xi'an 710065, China; 13571843652@163.com (Z.W.); 18710563168@163.com (S.Z.)

⁴ No.11 Oil Production Plant, Changqing Oilfield Company, PetroChina, Qingyang 745000, China; songtin_cq@petrochina.com.cn

* Correspondence: wangtong214@126.com

Abstract: The Ordos Basin has abundant resources in its tight sandstone reservoirs, and the use of well logging technology stands out as a critical element in the exploration and development of these reservoirs. Unlike conventional reservoirs, the commonly used interpretation models are not ideal for evaluating tight sandstone reservoirs through logging. In order to accurately evaluate parameters and identify fluid properties in the tight sandstone reservoirs of the Ordos Basin, we propose the adaption of conventional logging curves. This involves establishing an interpretation model that integrates the response characteristics of logging curves to tight sandstone reservoirs in accordance with the principles of logging. In this approach, we create interpretation models specifically for shale content, porosity, permeability, and saturation within the tight sandstone reservoir. Using the characteristics of the logging curves and their responses, we apply a mathematical relationship to link these parameters and create a template for identifying fluid properties within tight sandstone reservoirs. The average absolute errors of the new multi-parameter weighting method shale content interpretation model and porosity classification saturation interpretation model for quantitative evaluation of reservoir shale content and oil saturation are small, and the accuracy meets the production requirements. In this paper, the four-step method is used to identify the fluid properties of tight sandstone reservoirs step by step, which is to use the interrelationship between curves, eliminate the useless information, enhance the useful information, and finally solve the problem of identifying the fluid properties of tight sandstone reservoirs, which is difficult to identify, and realize the linear discrimination of the interpretation standard, which improves the accuracy of interpretation. The proven multi-information, four-step, step-by-step fluid property identification template has an accuracy of more than 90%. The interpretation model has been applied to 20 wells on the block with a compliance rate of 95.23%, providing the basis for accurately establishing the tight sandstone interpretation standard. The newly introduced log evaluation approach for tight sandstone reservoirs effectively overcomes the technical hurdles that have previously hindered the evaluation of such reservoirs in the Ordos Basin. This method is suitable for wide application and can be used for quantitative evaluation of tight sandstone reservoirs in different regions.

Keywords: tight sandstone; logging interpretation; model; fluid property identification; siliciclastic reservoirs; unconventional petroleum resources



Citation: Xu, B.; Wang, Z.; Song, T.; Zhang, S.; Peng, J.; Wang, T.; Chen, Y. Modeling of Quantitative Characterization Parameters and Identification of Fluid Properties in Tight Sandstone Reservoirs of the Ordos Basin. *Processes* **2024**, *12*, 278. <https://doi.org/10.3390/pr12020278>

Academic Editors: Dicho Stratiev and Qingbang Meng

Received: 15 December 2023

Revised: 20 January 2024

Accepted: 25 January 2024

Published: 26 January 2024



Copyright: © 2024 by the authors. Licensee MDPI, Basel, Switzerland. This article is an open access article distributed under the terms and conditions of the Creative Commons Attribution (CC BY) license (<https://creativecommons.org/licenses/by/4.0/>).

1. Introduction

As global unconventional oil and gas exploration and development rapidly progresses, scientists are increasingly focusing on the development of tight sandstone reservoirs.

Effective identification of fluids in these reservoirs is considered to be the first and crucial step for their efficient development [1,2]. Accurate identification of fluids in tight sandstone reservoirs is of great importance to the overall development of such reservoirs [3]. China's land-phase tight sandstones are generally characterized by tight lithology and strong heterogeneity, making it difficult for conventional logging techniques to be useful for fluid identification [4,5]. Currently, logging curve identification for tight sandstones mainly includes lithology logging curves (natural potential SP, natural gamma GR), porosity logging curves (acoustic logging AC, density DEN, neutron CN), and resistivity logging curves (microlateral MLL, octolateral LL8, etc.) [6,7]. Based on the above logging curves for pore fluid identification, the selection of logging curves needs to be optimized and standardized [8,9].

The Ordos Basin is located at the intersection of the stable zone in eastern China and the active zone in western China. It is surrounded by multiple rifts as shown in Figure 1 [10]. Internally, the basin has a generally smooth structure characterized by a dip angle of less than 1° . The tectonic structure is simple, with gentle tectonics, stable subsidence, minimal fracturing and low activity [11,12]. The basin can be divided into six primary tectonic units: the northern Yimeng uplift, the western thrust belt, the western Tianhuan depression, the central Yishan slope, the southern Weibei uplift, and the eastern Jinxi fault fold belt [13].

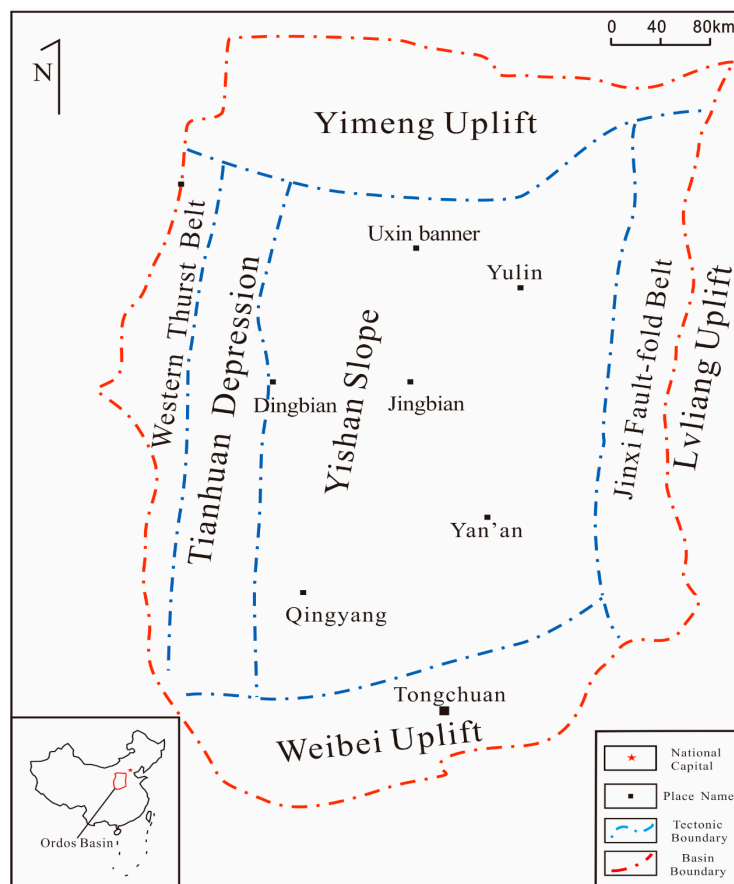


Figure 1. Highly generalized tectonic map of the Ordos Basin study area.

Tight sandstone reservoirs in the Ordos Basin exist mainly in the lower assemblage, especially in the Chang 7–Chang 10 section [14]. These reservoirs exhibit poor physical properties, characterized by complex pore throat structure, pronounced heterogeneity, and complicated rock–electric relationships [15,16]. There are the following difficulties in logging interpretation: the interpretation model based on the relationship study of the “four properties” (lithological characteristics, physical characteristics, electrical characteristics and oil-bearing characteristics) of the conventional reservoir cannot effectively meet the

evaluation of logging in tight sandstone reservoirs [17–19]. Due to the influence of the sandstone skeleton, the contribution of fluid properties to well logging information in tight sandstone reservoirs is much smaller than that of the rock skeleton, making it difficult to discriminate fluid properties [20]. Therefore, the results of well logging interpretation in tight sandstones are not satisfactory [21,22]. Aiming at the problems of conventional logging curves on tight sandstone interpretation and evaluation, this paper starts from tight sandstone reservoirs in Ordos Basin and establishes or selects the interpretation model of the lithology, porosity, permeability and saturation of tight sandstone reservoirs according to the four properties of reservoirs and the logging principle. We then enhance the relevant signals within the log curves using the reflection of reservoir characteristics in the log curves, supplemented by oil test and recovery data. This process eliminates extraneous information to provide a standardized interpretation for distinguishing between oil and water reservoirs.

2. Characterization of Tight Sandstone Reservoirs

2.1. Lithological Characteristics

According to the thin section electron micrographs and core photographs of the lower assemblage core of the Yanchang Formation in the Ordos Basin (Figures 2 and 3), it can be seen that the pore type is dominated by intergranular pores, which are well developed. There are more fillers, mainly colluvium, and the colluvium is mainly illite and quartz, with better storage capacity. Combined with the petrographic description data of the logged wells, the main rock type of the lower assemblage of tight sandstone reservoirs is fine sandstone, with a small amount of medium sandstone and siltstone (Figure 4a). The mineralogical composition is dominated by feldspar sandstone (Figure 4b), with feldspar ranging from 55.13% to 83.54% of the fractions, with an average of 56.53%, quartz content ranging from 16.05% to 35.06%, with an average of 22.06%, and lithic content ranging from 3.66% to 10.71%, with an average of 5.61%. The variation in the lithology of the tight sandstone in the longitudinal direction is detailed in Figure 5. In the logging map, it can be seen that the lithology of the lower assemblage group is better, which is dominated by shaly sandstone and sandstone, and has better mining potential. Lower assemblage group tight sandstone casting thin section statistics are summarized in Table 1.

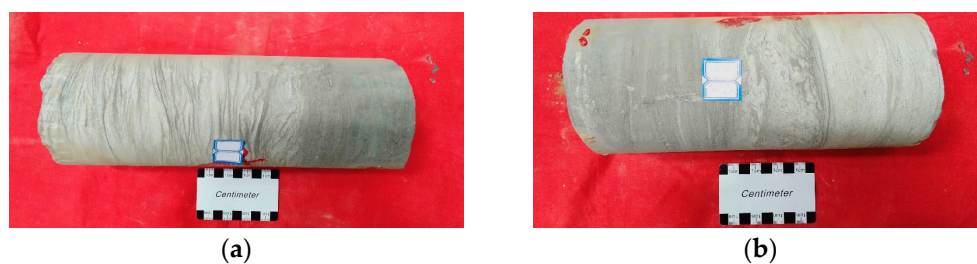


Figure 2. Photographs of tight sandstones of the lower assemblage of the Yanchang Formation. (a) Coring well L96, depth 1635 m, convolute bedding. (b) Coring well L108, depth 1508 m, convolute bedding.

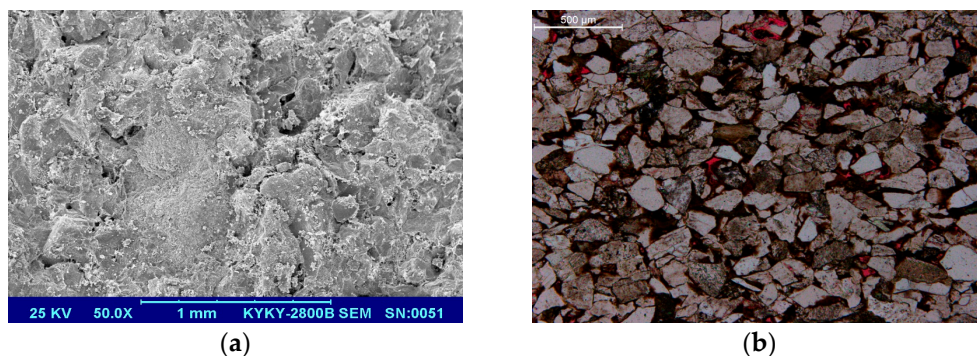


Figure 3. Pore characteristics of the lower assemblage tight sandstone of the Yanchang Formation. (a) Core electron microscope picture. (b) Picture of a thin section of a core cast.

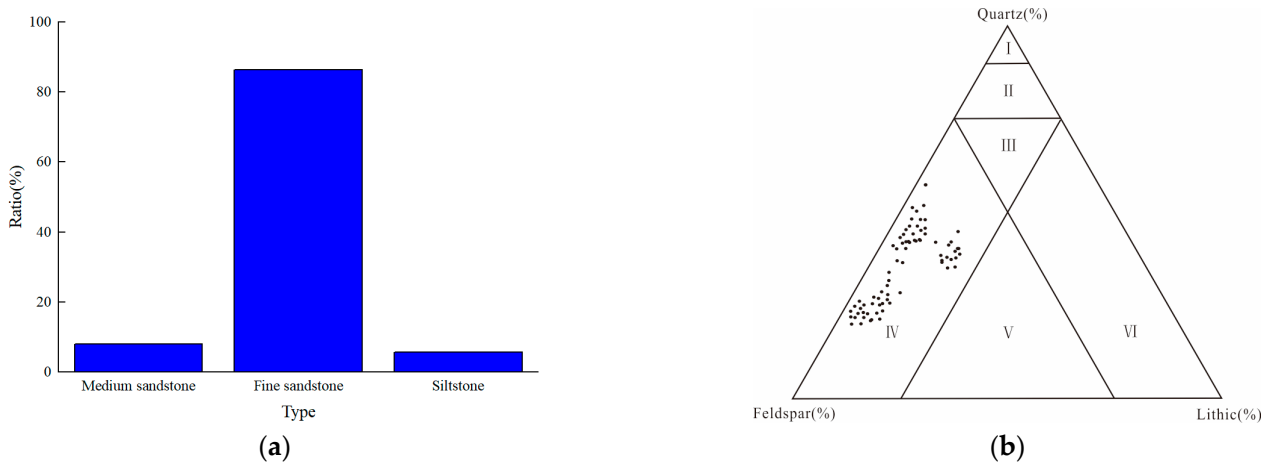


Figure 4. Sandstone lithology analysis diagram. (a) Sandstone lithology statistical histogram. (b) Sandstone compositional triangulation. I—Pure quartz sandstone; II—quartz sandstone; III—secondary lithic feldspar sandstone or secondary feldspar lithic sandstone; IV—feldspar sandstone; V—lithic feldspar sandstone or feldspar lithic sandstone; VI—lithic sandstone.

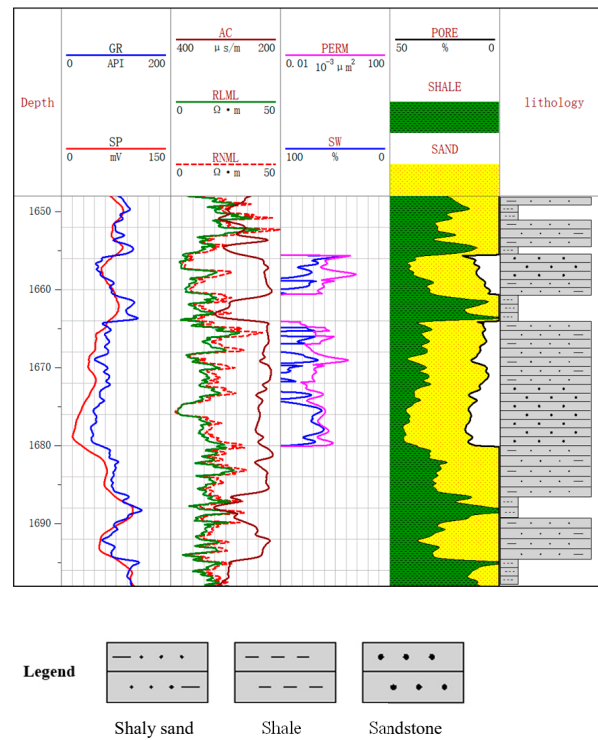


Figure 5. L110 well logging composite histogram.

2.2. Physical Characteristics

In logging, the physical properties of the reservoir are typically characterized using the porosity and permeability parameters. The analysis of porosity and permeability variation patterns is primarily based on data from 252 sandstone samples. According to the core analysis data, the porosity distribution interval from Chang 7 to Chang 9 ranges from 1.1% to 18.81% (Figure 6a), with an average of 8.33%, and the main distribution range is between 2% and 12%, accounting for 84.52% of the porosity samples in this interval. The distribution range of permeability is 0.01–37.71 × 10⁻³ μm² with a mean of 0.33 × 10⁻³ μm² (Figure 6b). The main distribution range of permeability is between 0.07 × 10⁻³ μm² and 0.4 × 10⁻³ μm², which accounted for 61.5% of the total number of samples, while samples between 0.01 × 10⁻³ μm² and 0.1 × 10⁻³ μm² accounted for 48% of the samples, samples

between 0.1 and $1 \times 10^{-3} \mu\text{m}^2$ accounted for 50.4% of the samples, and samples larger than $1 \times 10^{-3} \mu\text{m}^2$ accounted for only 1.6% of the total number of samples.

Table 1. Statistical table of cast thin section identification of tight sandstones of some lower assemblage group.

Core Samples	Well	Depth	Terrigenous Debris			Thin-Section Porosity (%)
			Quartz (%)	Feldspar (%)	Lithic (%)	
1	L96	1634.5	33.0	58.0	8.0	4
2	L108	1507.3	31.0	57.0	6.0	8
3	L108	1513.5	28.0	67.0	5.0	3
4	L71	1479.7	25.0	66.0	8.0	2
5	L120	1312.6	26.0	65.0	7.0	1
6	L92	1677.7	28.0	67.0	4.0	2
7	L92	1671.9	28.0	66.0	6.0	3
8	L92	1751.4	20.0	72.0	8.0	1
9	P198	1418.1	21.0	67.0	11.0	5
10	P198	1531.5	29.0	61.0	10.0	4
11	U113	1767	25.0	67.0	7.95	3
12	P200	1817.4	27.8	63.3	8.89	1
13	P200	1820.2	28.6	64.8	6.59	2
14	U129	1745.7	25.6	64.4	10.0	5
15	Q1	832.9	31.4	52.3	16.28	2
16	X105	1081.3	27.2	64.1	8.7	5
17	X105	1193.6	31.5	55.4	13.04	7
18	S1040	1080.2	28.2	64.7	7.06	2
19	S32	1471.5	21.7	72.3	6.0	8
20	S32	1553	23.3	66.3	10.4	3

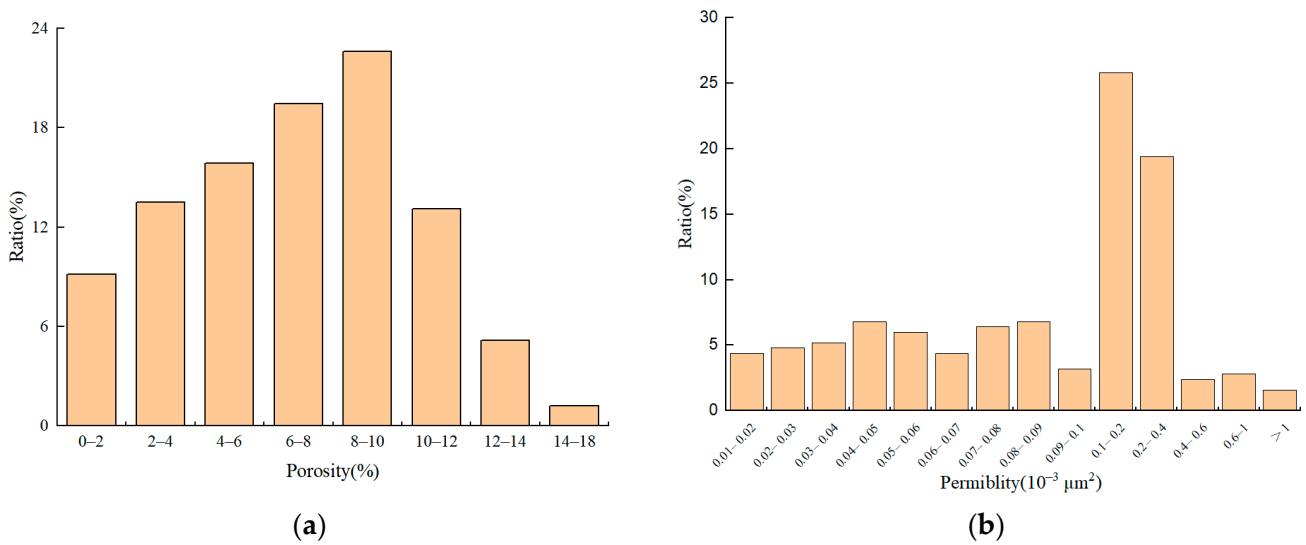


Figure 6. Physical characteristics distribution histogram. (a) Porosity distribution histogram. (b) Permeability distribution histogram.

2.3. Electrical Characteristics

Oil-bearing reservoirs in tight sandstones are characterized by low natural gamma, negative anomalies in natural potential, and high resistivity, and the resistivity of oil-bearing systems is generally greater than $20 \Omega\cdot\text{m}$ [23,24]. The layers with high shale content are all characterized by high natural gamma, small natural potential amplitude differences, relatively low resistivity, and high acoustic time difference values. As a whole, the resistivity of the tight sandstone reservoirs, on the other hand, is relatively high, ranging from $20 \Omega\cdot\text{m}$ to $50 \Omega\cdot\text{m}$ (Figure 7).

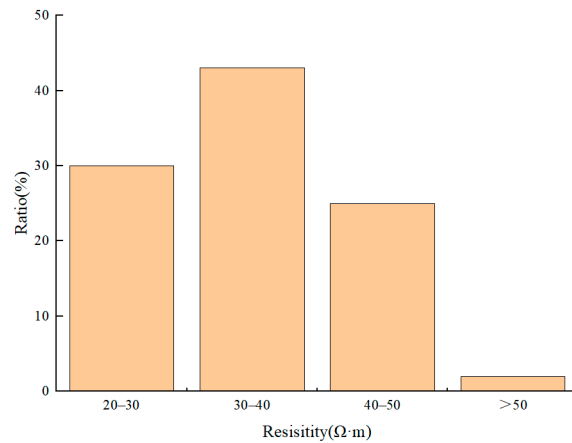


Figure 7. Resistivity distribution histogram.

2.4. Oil-Bearing Characteristics

The oil-bearing grades of tight sandstone reservoirs mainly have three grades: oil stains, oil traces and fluorescence, with oil stains accounting for 14.76%, oil traces accounting for 28.01% and fluorescence accounting for 26.36%. According to the statistics, the logging level of oil-producing reservoirs is generally above the oil trace, and the logging level above the oil trace accounts for 42.77% of the total number of wells (Figure 8a). The oil saturation is the calculated value from the logging, the distribution ranges from 2.52% to 40.81% and the average value is 20.81% (Figure 8b). From the distribution histogram, it can be seen that the distribution of oil saturation is mainly concentrated between 10% and 30%, accounting for 82.39% of the total number of samples, indicating that the tight sandstone reservoirs of the lower assemblage are not full of oil [25,26]. Higher resistivity values do not reflect the oil content but are more influenced by the rock skeleton. When calculating oil saturation in tight sandstone reservoirs, the original Archie model needs to be improved or a new oil saturation interpretation model needs to be established.

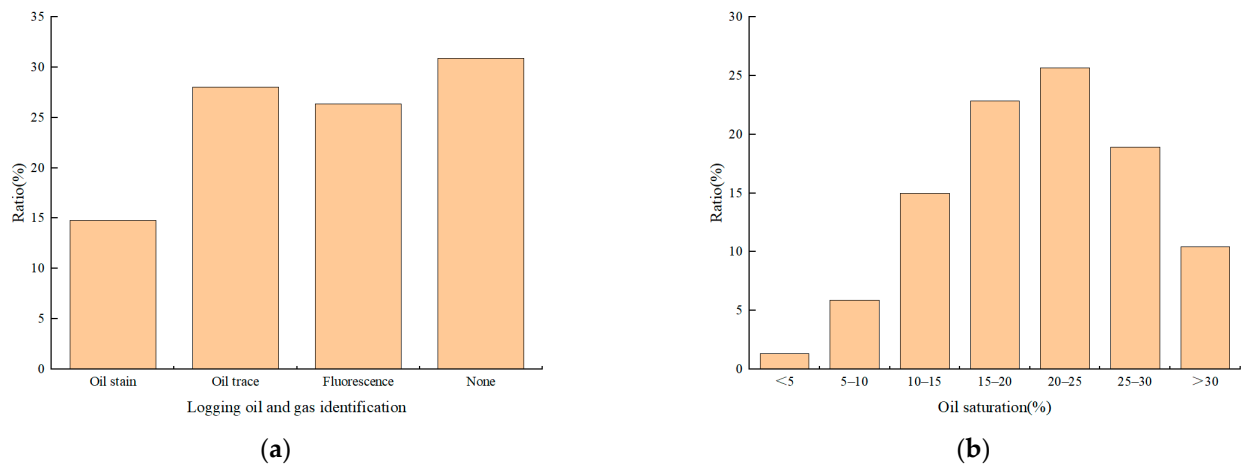


Figure 8. Oil-bearing characteristics distribution figure. (a) Logging grade distribution histogram. (b) Oil saturation distribution histogram.

3. Research on Evaluation Methods of Logging Interpretation

For fluid identification of tight sandstone reservoirs, it is necessary to first select the logging parameters of special areas in the reservoir and take this parameter as a standard [27]. Subsequently, by highlighting specific parameters in distinct areas, the reservoir characteristics become discernible and the influence of extraneous elements such as the rock skeleton can be minimized [28,29]. This approach facilitates rapid and accurate identification of fluid properties in tight sandstone reservoirs. In addition, variations in

pore structure, which affect the oil content and oil-bearing properties in tight sandstone reservoirs, also affect the fluid response characteristics to some extent [30]. According to the actual situation of tight sandstone reservoirs, the reservoir itself has a variety of characteristics, and using only a single parameter or a certain logging method will make it difficult to identify the fluid properties of tight sandstone reservoirs [31]. Based on this, when analyzing the fluid parameters in the reservoir, it is necessary to combine various factors in the reservoir with a comprehensive analysis; this optimization process allows refinement of the reservoir geological characteristics [32]. In the case of tight sandstones, there are numerous factors that affect the identification of the reservoir fluid, including shale content, porosity, permeability, and water saturation. The establishment of a logging interpretation model is especially important in the Lower Assemblage reservoir of the Ordos Basin, which is tight and whose fluid distribution is complicated [33,34].

3.1. Calculation of Shale Content

Usually, the interpretation of shale content in sandstone reservoirs is sought by GR and SP. However, the lithology of the tight sandstone reservoir is dominated by fine sandstone with small mean grain size and strong adsorption, which adsorbs certain radioactive materials, so the GR logging value is high [35]. In contrast, the shale content interpreted in terms of GR and SP is on the high side due to the poor physical properties of the tight sandstone reservoir and the reduced SP amplitude difference. To eliminate the influence of non-formation factors on the shale content evaluation, all logging curves are analyzed for shale content reflection in the reservoir and the logging principles are analyzed [36]. The acoustic propagation in the tight sandstone layer is affected by the lithology and the contact mode of the rock particles, the propagation mode is nonlinear, the acoustic time difference value decreases and the calculated shale content is small. Therefore, in order to reduce the error of the logging curve in calculating the shale content of tight sandstone reservoirs, a compensating acoustic curve is introduced to weight the shale index calculated by GR and AC (or SP and AC) to explain the shale content of tight sandstone reservoirs [37].

$$\Delta GR = \frac{GR - GR_{min}}{GR_{max} - GR_{min}} \quad (1)$$

ΔGR : natural gamma calculated shale index; GR : natural gamma logging value, API; GR_{min} : gamma value for pure sandstone, API; GR_{max} : gamma value for pure mudstone, API.

$$\Delta AC = \frac{AC - AC_{min}}{AC_{max} - AC_{min}} \quad (2)$$

ΔAC : compensated acoustic calculation of shale index; AC : compensated acoustic logging values, $\mu s/m$; AC_{min} : compensated acoustic value for pure sandstone, $\mu s/m$; AC_{max} : compensated acoustic value for pure mudstone, $\mu s/m$.

$$\Delta SP = 1 - \frac{\Delta SP_m}{\Delta SP_{sa}} \quad (3)$$

$$\Delta SP_m = SP_m - SP_{sh} \quad (4)$$

$$\Delta SP_{sa} = SP_{sa} - SP_{sh} \quad (5)$$

ΔSP : natural potential calculated shale index; SP_m : measured actual natural potential of sandstone, mV; SP_{sh} : measured natural potential of mudstone, mV; SP_{sa} : natural potential value of water-bearing pure sandstone, mV.

$$SH = (1 - K) \times \Delta GR + K \times \Delta AC \quad (6)$$

$$SH = (1 - K) \times \Delta SP + K \times \Delta AC \quad (7)$$

$$V_{sh} = \frac{2^{GCUR \times SH} - 1}{2^{GCUR} - 1} \quad (8)$$

SH: shale index, radix; *K*: weighting factor; *GCUR*: the lithology coefficient, for older formations is 2 and for newer formations is 3.7.

3.2. Calculation of Porosity

For the interpretation of porosity, the Wiley model derived from the time-averaged formula is generally used, but tight sandstone reservoirs, with complex pore structures and nonlinear propagation of acoustic waves in the formation, have higher error in the porosity calculated by the Wiley model based on the time-averaged formula [38]. In 1986, three Raymer–Hunt–Gardner logging analysts of the French TOTAL Petroleum Company, after a thorough study of the work of their predecessors, took into account the influence of pore structure on acoustic wave propagation and proposed the formula of the acoustic formation factor, which is found to be modeled by Raymer–Hunt–Gardner through a comparative analysis [39,40]. The accuracy of porosity interpretation in tight sandstone reservoirs is significantly superior to that of the Wylie model. Therefore, the Raymer–Hunt–Gardner model is selected for porosity calculation in tight sandstone reservoirs:

$$\Delta AC_{CC} = \Delta AC - V_{sh} \times (\Delta AC_{sh} - \Delta AC_{ma}) \quad (9)$$

$$C = \frac{\Delta AC_{ma}}{(2 \times \Delta AC_f)} \quad (10)$$

$$\Phi_e = 1 - C - \sqrt{C^2 - \frac{\Delta AC_{ma}}{\Delta AC_f} + \frac{\Delta AC_{ma}}{\Delta AC_{CC}}} \quad (11)$$

ΔAC_{cc} : corrected acoustic time difference value, $\mu\text{s}/\text{m}$; *C* is a constant and is the reciprocal of the coefficient of skeletal lithology; ΔAC_{sh} : mudstone acoustic time difference, $\mu\text{s}/\text{m}$; ΔAC_{ma} : rock skeleton acoustic time difference, $\mu\text{s}/\text{m}$; ΔAC_f : pore fluid acoustic time difference, $\mu\text{s}/\text{m}$; Φ_e : effective porosity of rock, *f*.

3.3. Calculation of Permeability

Permeability determines the capacity of the reservoir and is a very important parameter in logging evaluation, but it is also the most difficult geological parameter to calculate accurately [41]. At present, the logging calculation of permeability generally adopts the empirical formula proposed by Timur, and in different blocks, the corresponding coefficients and indices of the empirical formula are determined [42,43]. In tight sandstone reservoirs, the correlation between permeability and porosity may decrease, but, overall, it remains positively correlated with porosity and negatively correlated with bound water saturation. The empirical formula for permeability calculation is still followed here, using the porosity of the tight sandstone in the lower assemblage of the study area. Permeability and bound water saturation data and the coefficients and exponents of the empirical formula are determined by the fitting method, and bound water saturation can be derived from conventional logging curves.

$$K = 0.126 \times \frac{\Phi^{0.08}}{S_{wi}^{1.11}} \quad (12)$$

K: permeability, $10^{-3} \mu\text{m}^2$; Φ : porosity, *f*; S_{wi} : bound water saturation, *f*.

3.4. Calculation of Oil Saturation

Oil saturation is the core of logging interpretation, and the commonly used oil saturation formula is Archie's formula and its improved type [44]. To improve the accuracy of saturation interpretation, it is necessary to have accurate cementation index *m*, saturation index *n*, and saturation constants *a* and *b*. According to the petrographic experimental data, the appropriate way to correct the petrographic parameters in Archie's formula was

elucidated, which can better control the accuracy of saturation calculation [45]. Through the analysis of the porosity–formation factor cross plot, it is found that all the data become two trends with a porosity of 7.1% as the demarcation; thus, here, according to the size of porosity, the rock electrical data are categorized, and the values of a , b , m and n are obtained, respectively, in order to improve the interpretation accuracy of oil saturation in tight sandstone reservoirs.

$$S_w = \sqrt[n]{\frac{a \times b \times R_w}{\Phi \times R_t^m}} \quad (13)$$

$$S_o = 1 - S_w \quad (14)$$

S_w : water saturation, f ; S_o : oil saturation, f ; a , b : lithological constants, dimensionless; m : lithological index, dimensionless; n : saturation index, dimensionless; R_w : formation water resistivity, $\Omega \cdot m$; R_t : formation true resistivity, $\Omega \cdot m$; Φ : porosity, f .

3.4.1. Porosity Classification Method for Calculating Oil Saturation

Firstly, the sandstone samples of the lower assemblage are selected, the resistivity value of the rock samples is measured, combined with the formation water resistivity R_w , the formation factor F is found, and the m -value and a -value are obtained using regression analysis; the centrifugal method is used to measure the saturation and resistivity under different centrifugal speeds, and the power function relationship is established by the cross plot of the resistivity coefficients with the water-bearing saturation degree, so that the n -value and b -value can be determined.

Based on the porosity–formation factor cross plot, the data are categorized according to the porosity of 7.1%. When the porosity $\Phi \geq 7.1\%$, the corresponding rock electrical parameters $a = 1.320$, $b = 1.0705$, $m = 1.736$, $n = 1.629$ are calculated based on the relationship between porosity and formation factors and the relationship between water saturation and the resistivity index (Figure 9).

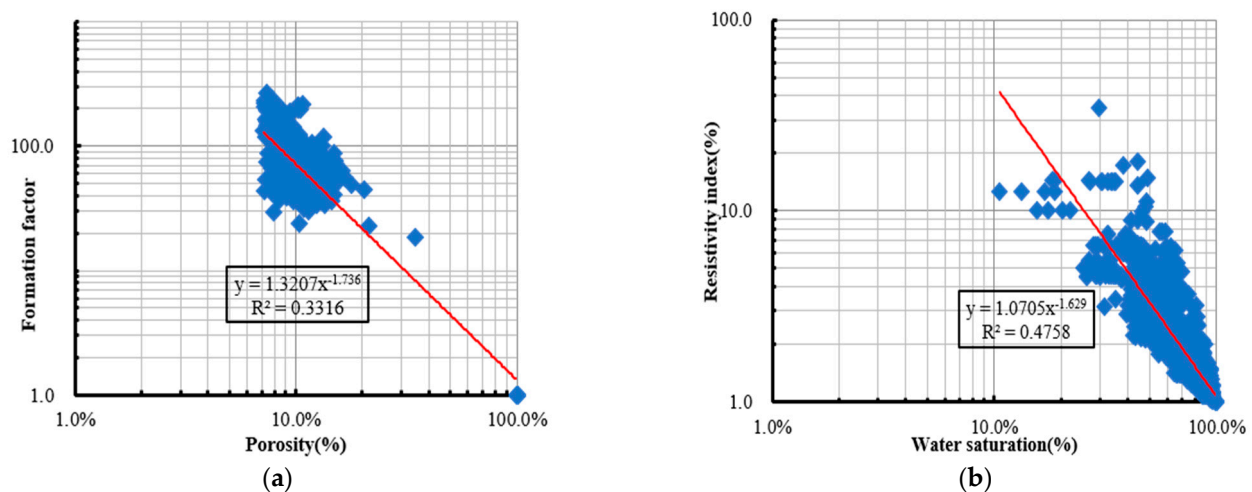


Figure 9. The relevant parameter cross plot when the porosity $\geq 7.1\%$. (a) Porosity and formation factor cross plot. (b) Water saturation and resistivity index cross plot.

When the porosity $\Phi < 7.1\%$, the rock electrical parameters $a = 1.8751$, $b = 1.1749$, $m = 1.297$, $n = 1.872$ are determined in the same way (Figure 10).

3.4.2. Calculation of Oil Saturation by Acoustic Time Difference Logging

When the interplay between the “four properties” of the reservoir is examined, it becomes clear that in tight sandstone reservoirs, resistivity does not accurately reflect the oil-bearing nature of the reservoir. Consequently, using the resistivity curve to calculate reservoir oil saturation results in significant errors [46]. The logging curve is a comprehen-

sive reflection of formation information, and the acoustic time-difference logging curve value contains formation skeleton information and porosity information, which in turn contains water-bearing porosity and oil-bearing porosity, and according to the definition of oil-bearing saturation, the ratio of oil-bearing porosity to total porosity is oil-bearing saturation [47]. Therefore, it is possible to build a volumetric model from the logging principle of compensated acoustic waves, convert it into a mathematical model, remove invalid information, extract the required information, and build a calculation model for oil bearing saturation (Figure 11).

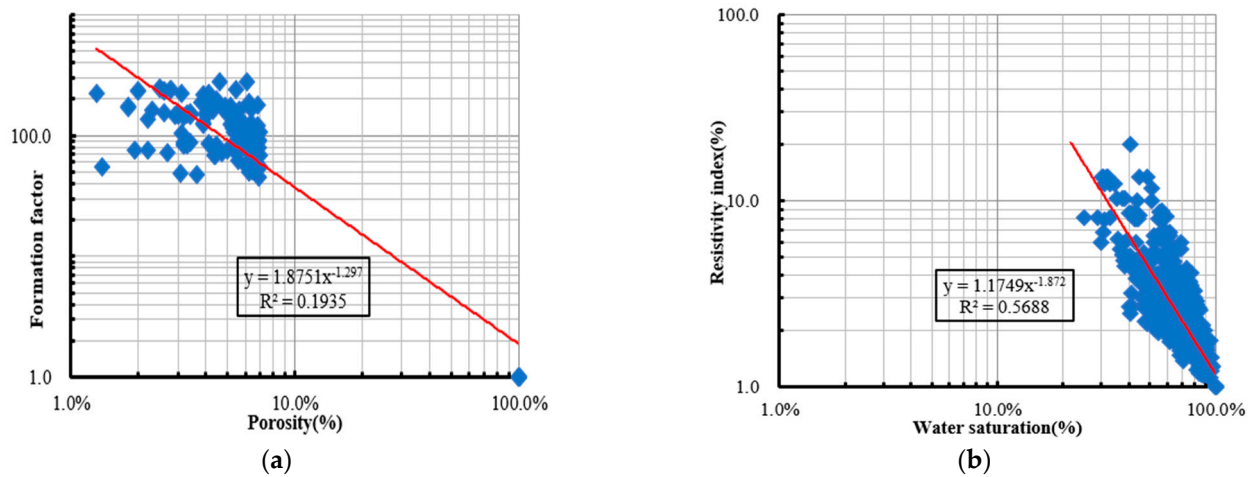


Figure 10. The relevant parameter cross plot when the porosity <7.1%. (a) Porosity and formation factor cross plot. (b) Water saturation and resistivity index cross plot.

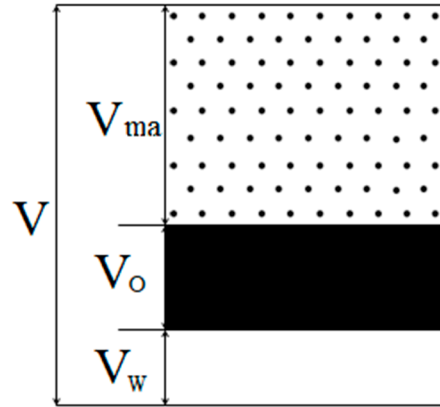


Figure 11. Volumetric modeling for calculating oil bearing saturation.

The acoustic logging volume model is converted into an equivalent model to establish the relationship between each parameter, and the mathematical relationship equation between porosity and acoustic time difference is as follows:

$$AC = AC_{ma} \times (1 - \Phi_w - \Phi_o) + AC_o \times \Phi_o + AC_w \times \Phi_w \tag{15}$$

It is known from the definition of porosity that the total porosity is the sum of oil-bearing porosity and water-bearing porosity of the formation; therefore:

$$\Phi = \Phi_o + \Phi_w \tag{16}$$

This is then finalized according to the definition of oil-bearing saturation:

$$S_o = \frac{(AC - AC_{ma})}{(AC_o - AC_w) \times \Phi} - \frac{(AC_w - AC_{ma})}{(AC_o - AC_w)} \tag{17}$$

AC: acoustic time difference logging value, $\mu\text{s}/\text{m}$; AC_w : sonic value of formation water at formation condition, $\mu\text{s}/\text{m}$; AC_o : acoustic wave value of crude oil under formation conditions, $\mu\text{s}/\text{m}$; AC_{ma} : acoustic value of sandstone skeleton, $\mu\text{s}/\text{m}$; Φ_w : water-bearing porosity, f; Φ_o : oil bearing porosity, f; Φ : total porosity of formation, f.

4. Fluid Property Identification

Reservoir lithology, physical properties and oil-bearing aspects are inherently inter-related and mutually constraining. The logging curve serves as a comprehensive representation of the lithological, physical, and petrophysical properties. In tight sandstone reservoirs, the proportion of fluid in the logging response is reduced, making it difficult for the resistivity curve, which is optimal for reflecting fluid properties, to comprehensively and accurately represent the oil-bearing situation of the formation [48].

The cross-plot method is to select the pairs of logging parameters and draw a cross plot to classify the fluid properties. As mentioned above, the logging parameters such as GR, RT and AC can distinguish oil and water layers and can be used to construct a cross plot to semi-quantitatively identify the fluid properties of the lower assemblage tight reservoir, targeting the geological and logging characteristics of tight sandstone reservoirs, focusing on extracting oil-bearing information from logging signals, synthesizing and enhancing useful information, and eliminating factors that affect the identification of oil-bearing properties. The reservoir fluid properties are progressively recognized through four steps. Using the oil test data of the study area (Table 2), combined with the GR, AC, and RILD values of the test oil test formation, AC/GR-RILD, AC-RILD, GR-AC*RILD/100, and AC-GR*RILD/100 cross plots are made, respectively (Figure 12). The above steps lead to the final identification of fluid properties.

Table 2. Fluid identification data for some lower assemblage group tight sandstones.

Well	GR/ API	AC/ $\mu\text{s}/\text{m}$	AC/GR	RILD / $\Omega\cdot\text{m}$	RILM / $\Omega\cdot\text{m}$	LL8 / $\Omega\cdot\text{m}$	Explanation of Conclusions
L77	94.45	243.41	2.58	43.29	43.48	56.28	O/W
L76	88.81	234.33	2.64	30.08	35.43	44.16	O/W
L63	99.32	282.68	2.85	63.56	64.96	130.25	O/W
L63	100.19	263.09	2.63	28.61	26.54	66.24	O/W
L89	95.2	269.14	2.83	42.18	57.61	166	O/W
L78	78.85	236.09	2.99	32.29	32.95	58.19	O/W
L128	50.23	238.46	4.75	28.2	27.45	34.1	O/W
L72	63.35	240.66	3.80	30.43	30.69	31.74	O/W
L109	77.93	238	3.05	28.06	29.98	35.41	O/W
L139	82.03	245	2.99	35.33	33.4	58.08	O/W
L183	73.64	241.75	3.28	70.29	68.74	63.1	O/W
L232	77.76	242.25	3.12	40.78	34.42	43.9	O/W
L233	84.02	235.14	2.80	99.03	65.62	103.89	WWO
L252	84.78	241.46	2.85	75.92	55.29	96.33	WWO
L251	76.41	222	2.91	41.02	49.63	68.6	WWO
L261	73.66	220.25	2.99	45.89	53.03	119.85	WWO
L46	82.55	230.06	2.79	20.13	22.99	24.6	WWO
L37	67.63	247.32	3.66	27.53	30.39	38.09	WWO
L43	81.19	223.08	2.75	44.9	54.08	55.15	WWO
L47	68.87	231.65	3.36	21.5	22.72	21.79	WWO
L55	79.76	233.46	2.93	27.79	26.94	31.81	W
L41	83.01	232.4	2.80	16.44	19.85	21.66	W
L76	59.38	262.63	4.42	13.73	13.74	15.83	W
L40	81.65	237	2.90	22.85	23.49	29.95	W
L75	87.62	235.58	2.69	26.26	30.21	56.54	W
L63	83.44	227.09	2.72	14.84	14.44	11.91	W
L74	98.25	255.24	2.60	67.58	60.05	47.88	W
L50	85.44	211.16	2.69	34.47	38.31	75.8	D
L51	108.62	255.48	2.35	46.86	59.97	60.05	D
P23	104.9	228.34	2.18	45.69	37.3	86.7	D
L80	99	231.5	2.34	20.98	25.26	32.35	D

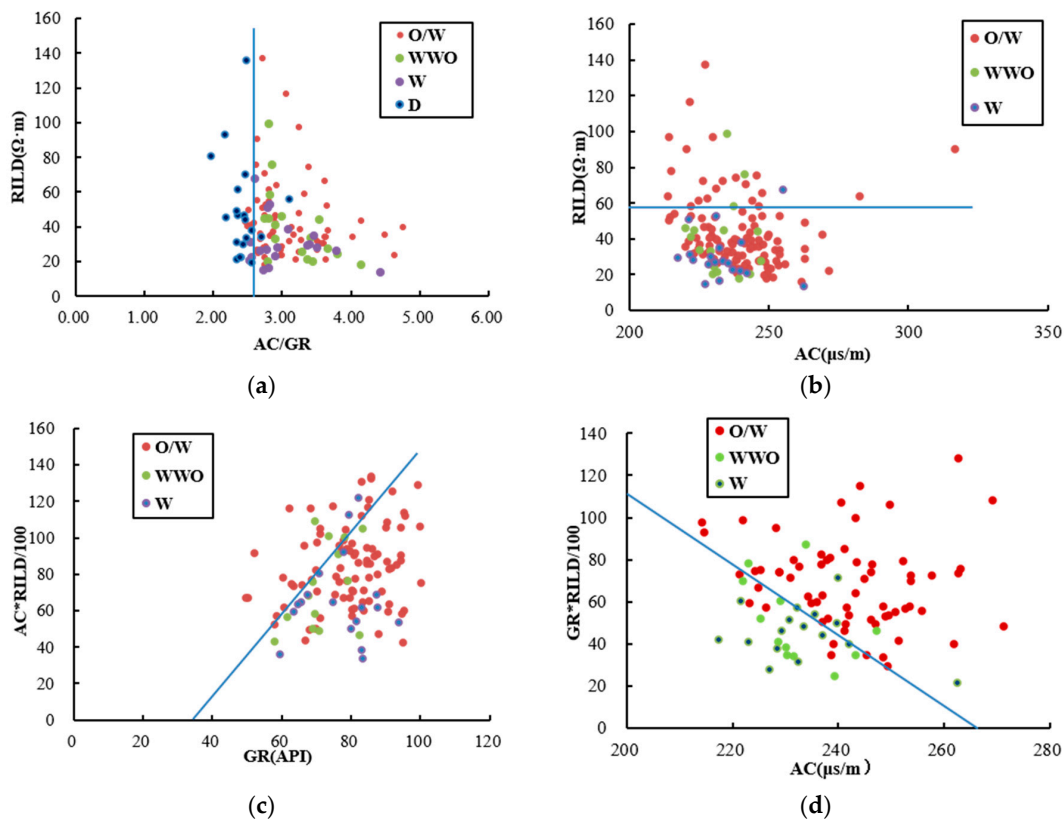


Figure 12. Logging fluid identification cross plot. (a) AC/GR-RILD cross plot. (b) AC-RILD cross plot. (c) GR-AC*RILD/100 cross plot. (d) AC-GR*RILD/100 cross plot.

In the first step, the AC/GR-RILD cross plot is generated, and if $AC/GR < 2.54$, the formation is dry, the dry layer of the tight sandstone reservoir is effectively identified, and the identified dry layer(D) data are removed.

In the second step, the remaining data are used to produce AC-RILD cross plot; if $RILD \geq 58 \Omega \cdot m$, the formation is an oil–water layer (O/W), the fluid properties of some layers can be identified, and the identified oil–water layer data are removed.

In the third step, the remaining data are used to generate the GR-AC*RILD/100 cross plot; if $AC*RILD/100 > 2.6*GR-91.31$, the reservoir is an oil–water layer, and the reservoir data with identified fluid properties are removed again.

In the fourth step, the AC-GR*RILD/100 cross plot is made with the remaining data; if $GR*RILD/100 \geq 110.5-0.41*AC$, the reservoir is an oil–water layer, and the remaining reservoirs are water layers (W) and water with an oil layer (WWO).

The oil–water layer identification template established in four steps is used to finalize a linear discrimination criterion for oil–water layers:

When $AC/GR < 2.54$, the reservoir is a dry layer.

Condition 1: $RILD \geq 58 \Omega \cdot m$;

Condition 2: $AC*RILD/100 \geq 2.6*GR-91.31$;

Condition 3: $GR*RILD/100 \geq 110.5-0.41*GR$.

If any one of conditions 1–3 is satisfied, the reservoir is an oil–water layer; otherwise, the reservoir is a water layer.

According to the statistical statistics, it is concluded that the accuracy of the fluid property identification template or linear discriminating criterion established by the four-step method to discriminate the fluid properties of tight sandstone is over 93.29%.

5. Examples of Logging Interpretation Model Applications

Using the newly constructed lithology, porosity, permeability and saturation interpretation model and interpretation standard, 20 wells in the study area are secondarily

interpreted, and the interpretation error of each parameter is less than 5%, with 95.23% agreement between the interpretation conclusion and the oil test conclusion (Table 3).

Table 3. Comparison of model interpretation results with actual interpretation findings.

Well	GR/ API	AC/ $\mu\text{s/m}$	RILD / $\Omega\cdot\text{m}$	POR /%	PERM / $10^{-3} \mu\text{m}^2$	SW /%	Oil Test (m^3)		Explanation of Conclusions	Explanatory Model				
							Oil	Water		Condition 1	Condition 2	Condition 3	Result	
L108	62.29	238.09	22.04	13.37	0.36	58.96	2.04	19.86	O/W				yes	O/W
L34	78.12	232.58	38.03	10.35	0.52	55.32	1	2.6	O/W				yes	O/W
L80	75.29	246.61	58.46	14.03	1.47	30.72	1.83	1.84	O/W	yes				O/W
L96	70.42	251.82	42.41	15.63	1.99	33.35	1.58	0.73	O/W		yes			O/W
L110	78.22	253.54	33.64	15.95	0.95	37.64	0.87	1.78	O/W				yes	O/W
L121	78.08	253.00	21.89	15.37	1.66	50.96	3	0.4	O/W				yes	O/W
L128	53.95	244.83	32.30	15.60	1.19	39.50	2.7	5.63	O/W		yes			O/W
L71	80.61	245.25	36.15	12.83	0.78	45.17	1	5	O/W				yes	O/W
L92	64.25	231.17	13.27	11.36	0.16	95.10	/	/	W					W
L120	84.34	222.03	116.27	6.73	8.53	22.55	0.49	1.83	O/W	yes				O/W
P198	67.30	211.74	30.43	6.34	0.07	45.52	2	1	O/W				yes	O/W
P200	89.89	217.87	19.29	7.07	0.77	56.00	1.6	7	O/W				yes	O/W
P201	83.45	259.12	29.56	16.52	1.26	39.12	1.1	5.62	O/W				yes	O/W
U113	77.12	253.07	43.14	15.83	1.76	32.56	5	8	O/W				yes	O/W
U127	82.73	225.17	30.36	7.81	0.20	85.75	0	31.55	W				yes	O/W
U129	62.46	221.44	52.30	9.01	1.08	52.78	1.3	1.8	O/W		yes			O/W
Q1	85.89	216.10	25.89	6.66	0.28	60.15	1.4	2.88	O/W				yes	O/W
X105	62.22	233.50	44.04	12.12	0.74	42.76	5.9	9	O/W		yes			O/W
S1040	85.03	230.08	40.22	9.67	0.40	48.18	0.94	2.231	O/W				yes	O/W
S32	80.59	243.50	20.69	13.27	0.36	51.72	3.67	5.403	O/W				yes	O/W

Figure 13 shows a graph of the interpreted results for the L110 well. The interpreted porosity, permeability and oil-bearing saturation are close to the core analysis values. The logging depth is 1672–1680 m. The natural potential and natural gamma curve characteristics are consistent with the lithological characteristics of the sandy mudstone profile and the RLL8, RILM and RILD logging curve characteristics are consistent with the oil and water formations identified by the logging interpretation. Resistivity averages 32.7 $\Omega\cdot\text{m}$, porosity averages 9.96 PU, permeability is $0.87 \times 10^{-3} \mu\text{m}^2$ and oil saturation is 51.3%. It can be seen from the shot hole layer that after the layer was put into production, the initial production of liquid was 8.33 m^3 , oil production was 2.70 t, and water bearing was 67.59%, which is an oil and water layer, which is consistent with the interpretation results.

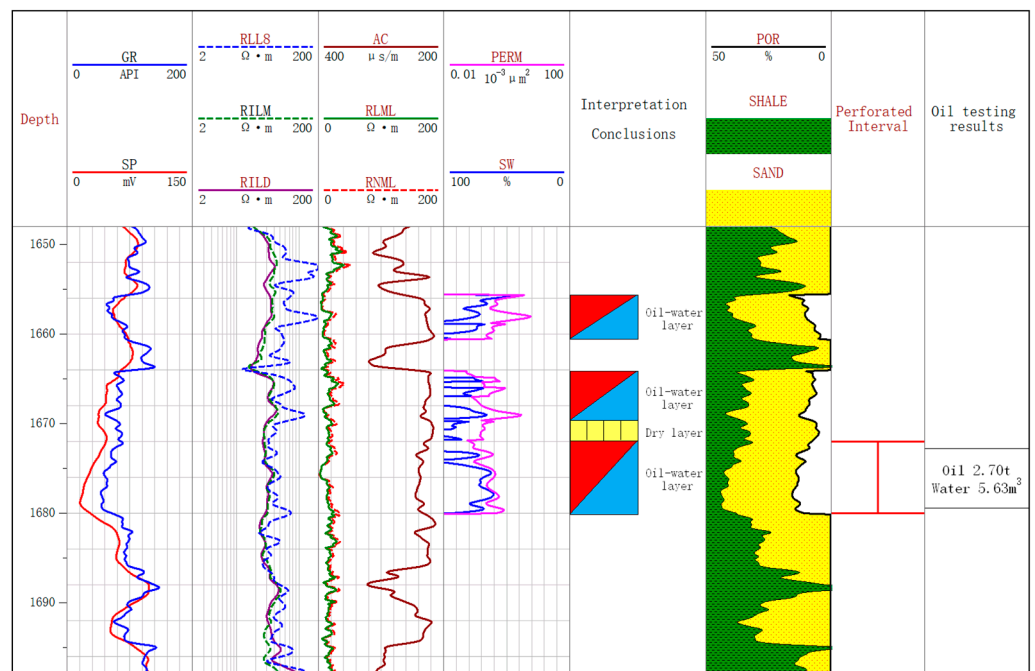


Figure 13. Comprehensive histogram of L110 logging interpretation.

6. Conclusions

- (1) The investigation of the evaluation method for tight sandstone reservoirs in the lower assemblage of the south-central Ordos involves the exploration of the interrelationships among the “four properties”. Based on this research, specialized models focusing on parameters such as the shale content, porosity, permeability, and saturation degree of tight sandstone reservoirs are developed or selected. These models demonstrate effective applicability to tight sandstones.
- (2) For the problem of high shale content in tight sandstone reservoirs, GR and AC (SP and AC) are used to calculate the shale index, and the weighting method is effective.
- (3) The established porosity classification method and acoustic time difference method for calculating oil saturation in tight sandstone reservoirs overcame the difficulty of resistivity reflecting the weakening of oil bearing and improved the accuracy of interpretation of oil saturation in reservoirs.
- (4) The multi-information four-step method gradually recognizes the fluid characteristics of tight sandstone reservoirs and improves the compliance rate of log interpretation, which is applied to 20 wells in the block with a compliance rate of 95.23%, and lays the foundation for accurately establishing the interpretation standard of tight sandstone. This method is not only important for the development of tight sandstone reservoirs in the lower assemblage of the Ordos Basin but also for the identification of fluid properties of tight sandstone reservoirs in other blocks.

Author Contributions: Writing—original draft: B.X.; writing—review and editing: Z.W. and T.W.; methodology: B.X. and T.S.; validation: S.Z. and J.P.; formal analysis: T.S. and Y.C. All authors have read and agreed to the published version of the manuscript.

Funding: This research received no external funding.

Data Availability Statement: We state that the data are unavailable due to privacy or ethical restrictions of the company and university.

Conflicts of Interest: Authors Zhenhua Wang, Shuxia Zhang were employed by the company Research Institute of Shannxi Yanchang Petroleum (Group) Co., Ltd. Author Ting Song was employed by the Changqing Oilfield Company. The remaining authors declare that the research was conducted in the absence of any commercial or financial relationships that could be construed as a potential conflict of interest.

References

1. Zhou, L.H.; Chen, C.W.; Han, G.M.; Yang, F. Difference characteristics between continental shale and tight oil and exploration practice: A case from Huanghua Depression, Bohai Bay Basin. *Earth Sci.* **2021**, *46*, 555–571.
2. Huang, W.; Zhang, X.L.; Zhao, J.Y. Fluid Identification of Tight Reservoir in Chang 9 Formation, Ordos Basin. *J. Northwest Univ.* **2015**, *45*, 811–818.
3. Wen, B.; Zhou, Y. Study on fluid identification of low porosity and low permeability reservoir. *Petrochem. Ind. Technol.* **2017**, *24*, 126.
4. Albrecht, D.; Reitenbach, V. Laboratory measurements of fluid transport properties on tight gas sandstones and applications. *Energy Procedia* **2014**, *59*, 366–373. [[CrossRef](#)]
5. Bi, M.W.; Chen, S.Y.; Zhou, Z.H. Genesis of secondary pores of tight sandstone reservoir in He 8th Member in Su 6 area of Sulige gas field. *J. China Univ. Petrol.* **2015**, *39*, 8–16.
6. Guo, J.; Ling, Z.; Xu, X.; Zhao, Y.; Yang, C.; Wei, B.; Zhang, Z.; Zhang, C.; Tang, X.; Chen, T.; et al. Saturation Determination and Fluid Identification in Carbonate Rocks Based on Well Logging Data: A Middle Eastern Case Study. *Processes* **2023**, *11*, 1282. [[CrossRef](#)]
7. Bi, L.R.; Mao, Z.Q.; Xiao, C.W.; Liu, X.L. Application of normal distribution method in identifying oil (gas) and water zones. *J. Oil Gas Technol.* **2006**, *28*, 76–78.
8. Cheng, X.Z.; Zhou, C.C.; Fan, Y.R.; Wang, Z.H.; Huang, S.X. Genesis and identification of low contrast pay zones in fresh-water reservoirs. *J. Oil Gas Technol.* **2007**, *29*, 62–68.
9. Li, L.; Yuan, Z.; Hui, K.; Liu, S. Accumulation regularity of Upper Paleozoic gas in north Ordos Basin. *Oil Gas Geol.* **2000**, *21*, 268–271.

10. He, X.; Chen, S.; Hu, C.; Zhang, H.; Mou, F.; Dai, L.; Lu, Y.; Fu, X.; Han, M. Pore Structure Change in the Continental Shale Oil Reservoir and Its Main Influencing Factors: A Case Study of the Chang 7 Member in the Ordos Basin. *Processes* **2023**, *11*, 2314. [[CrossRef](#)]
11. Zhu, H.; Chen, K.; Liu, K.; He, S. A sequence stratigraphic model for reservoir sand-body distribution in the Lower Permian Shanxi Formation in the Ordos Basin, northern China. *Mar. Pet. Geol.* **2008**, *25*, 731–743. [[CrossRef](#)]
12. Chen, Z.; Li, X.; Chen, H.; Duan, Z.; Qiu, Z.; Zhou, X.; Hou, Y. The Characteristics of Lithofacies and Depositional Model of Fine-Grained Sedimentary Rocks in the Ordos Basin, China. *Energies* **2023**, *16*, 2390. [[CrossRef](#)]
13. Zheng, W.; Hu, X.; Chen, S.; Liu, J.; Jia, C. Characteristics of sedimentary evolution in the Upper Paleozoic Daniudi Gasfield, Ordos Basin. *Acta Sedimentol. Sin.* **2015**, *33*, 306–313.
14. Mao, K.Y. Logs fluid typing methods and adaptive analysis of tight sandstone reservoir of Yingcheng formation in Lishu Fault. *Adv. Earth Sci.* **2016**, *31*, 1056–1066.
15. Jamil, M.; Siddiqui, N.A.; Rahman, A.H.B.A.; Ibrahim, N.A.; Ismail, M.S.B.; Ahmed, N.; Usman, M.; Gul, Z.; Imran, Q.S. Facies Heterogeneity and Lobe Facies Multiscale Analysis of Deep-Marine Sand-Shale Complexity in the West Crocker Formation of Sabah Basin, NW Borneo. *Appl. Sci.* **2021**, *11*, 5513. [[CrossRef](#)]
16. Jamil, M.; Siddiqui, N.A.; Usman, M.; Wahid, A.; Umar, M.; Ahmed, N.; Haq, I.U.; El-Ghali, M.A.K.; Imran, Q.S.; Rahman, A.H.A.; et al. Facies analysis and distribution of Late Palaeogene deep-water massive sandstones in submarine-fan lobes, NW Borneo. *Geol. J.* **2022**, *57*, 4489–4507. [[CrossRef](#)]
17. Sun, J.M.; Wei, X.H.; Chen, X.L. Fluid identification in tight sandstone reservoirs based on a new rock physics model. *J. Geophys. Eng.* **2016**, *13*, 526–535. [[CrossRef](#)]
18. Wang, F.; Yang, X.M.; Zhang, Y.H.; Bian, H.Y. Application of multi-algorithmic fusion methods to fluid identity in tight reservoir. *Prog. Geophys.* **2015**, *30*, 2785–2792.
19. He, M.; Gu, H.M.; Wan, H. Log interpretation for lithology and fluid identification using deep neural network combined with MAHAKIL in a tight sandstone reservoir. *J. Pet. Sci. Eng.* **2020**, *194*, 107498. [[CrossRef](#)]
20. Li, H.; Tang, H.M.; Qin, Q.R.; Zhou, J.L.; Qin, Z.J.; Fan, C.H.; Su, P.; Wang, Q.; Zhong, C. Characteristics, formation periods and genetic mechanisms of tectonic fractures in the tight gas sandstones reservoir: A case study of xujiahe formation in YB area, sichuan basin, China. *J. Pet. Sci. Eng.* **2019**, *178*, 723–735. [[CrossRef](#)]
21. Li, B.; Tan, M.J.; Zhang, H.T. Interpretation method of nuclear magnetic resonance dual-TW logging in oil-wet tight sandstone reservoirs. *Appl. Geophys.* **2020**, *5*, 796–808. [[CrossRef](#)]
22. Chen, J.; Xie, R.C.; Liu, C.C.; Duan, Y.; Li, H.; Xiang, Y. Logging fluid identification and quantitative evaluation of Jurassic tight sandstone gas reservoir in Zhongjiang gas field. *Nat. Gas Ind.* **2019**, *39*, 136–141.
23. Fu, L.; Qin, Z.; Xie, A.; Chen, L.; Li, J.; Wang, N.; Qin, Q.; Mao, K. The relation of the “four properties” and fluid identification of the carboniferous weathering crust volcanic reservoir in the Shixi Oilfield, Junggar Basin, China. *Front. Earth Sci.* **2022**, *10*, 983572. [[CrossRef](#)]
24. Zou, C.; Zhu, R.; Wu, S.; Yang, Z.; Tao, S.; Yuan, X. Types, characteristics, genesis and prospects of conventional and unconventional hydrocarbon accumulations: Taking tight oil and tight gas in China as an instance. *Acta Pet. Sin.* **2012**, *33*, 173–187.
25. Dai, J.; Ni, Y.; Wu, X. Tight gas in China and its significance in exploration and exploitation. *Pet. Explor. Dev.* **2012**, *39*, 277–284. [[CrossRef](#)]
26. Guo, X.; Liu, K.; Jia, C.; Song, Y.; Zhao, M.; Zhuo, Q.; Lu, X. Hydrocarbon accumulation processes in the Dabei tight-gas reservoirs, Kuqa Subbasin, Tarim Basin, northwest China. *AAPG Bull.* **2016**, *100*, 1501–1521. [[CrossRef](#)]
27. Wu, H.; Zhao, J.; Wu, W.; Li, J.; Huang, Y.; Chen, M. Formation and diagenetic characteristics of tight sandstones in closed to semi-closed systems: Typical example from the Permian Sulige gas field. *J. Pet. Sci. Eng.* **2020**, *199*, 108248. [[CrossRef](#)]
28. Shaogui, D.; Yiren, F.; Guoxin, L. Influence of formation water salinity on physical properties of argillaceous sandstone. *Well Logging Technol.* **2006**, *30*, 113–115.
29. Haiyong, M.; Lifa, Z.; Xiuqin, D. Hydrochemical characteristics and geological significance of the Chang 8 formation of the Yanchang Formation in Jiyuan area, Ordos Basin. *J. Northwest Univ.* **2013**, *43*, 253–257.
30. Fan, R.; Zhou, L.; Wu, J.; Zeng, T.; Zhou, X.F. Research on tight sandstone reservoir fluids identification in Xujiahe formation, northeastern Sichuan Basin. *Petrol. Geol. Recov. Effic.* **2015**, *22*, 67–71.
31. Mode, A.W.; Anyiam, O.A.; Aghara, I.K. Identification and petrophysical evaluation of thinly bedded low-resistivity pay reservoir in the Niger Delta. *Arab. J. Geosci.* **2014**, *8*, 2217–2225. [[CrossRef](#)]
32. Xu, Z.; Jiang, S.; Liu, L.; Wu, K.; Li, R.; Liu, Z.; Shao, M.; Jia, K.; Feng, Y. Natural gas accumulation processes of tight sandstone reservoirs in deep formations of Songliao Basin, NE China. *J. Nat. Gas Sci. Eng.* **2020**, *83*, 103610. [[CrossRef](#)]
33. Wang, Q.; Chen, D.; Wang, F.; Gao, X.; Zou, Y.; Tian, Z.; Li, S.; Chang, S.; Yao, D. Origin and distribution of an under-pressured tight sandstone reservoir: The Shaximiao Formation, Central Sichuan Basin. *Mar. Petrol. Geol.* **2021**, *132*, 121–128. [[CrossRef](#)]
34. Zhou, X.; Xu, G.; Cui, H.; Zhang, W. Fracture development and hydrocarbon accumulation in tight sandstone reservoirs of the Paleogene Huagang Formation in the central reversal tectonic belt of the Xihu Sag, East China Sea. *Pet. Explor. Dev.* **2020**, *47*, 499–512. [[CrossRef](#)]
35. Jia, J.; Yin, W.; Qiu, N.; Wang, G.; Ma, L.; Liu, Y.; Liu, N. Migration and accumulation of crude oil in Upper Triassic tight sand reservoirs on the southwest margin of Ordos Basin, Central China: A case study of the Honghe Oilfield. *Geol. J.* **2017**, *53*, 2280–2300. [[CrossRef](#)]

36. Yang, H.; Fu, J.; Wei, X.; Liu, X. Sulige field in the Ordos Basin: Geological setting, field discovery and tight gas reservoirs. *Mar. Pet. Geol.* **2008**, *25*, 387–400. [[CrossRef](#)]
37. He, Y.H.; Yang, X.; Wang, X.J.; Zhong, Z.Q.; Hou, D.J. Fluid identification in low permeability reservoir in Jiyuan area, Ordos Basin. *China Petrol. Explor.* **2016**, *21*, 110–115.
38. Wyllie, M.R.J.; Gregory, A.R.; Gardner, L.W. Elastic wave velocities in heterogeneous and porous media. *Geo-Physics* **1956**, *21*, 41–70. [[CrossRef](#)]
39. Raymer, L.L.; Hunt, E.R.; Gardner, J.S. An improved sonic transit time-to-porosity transform. In Proceedings of the SPWLA 21st Annual Logging Symposium, Lafayette, LA, USA, 8 July 1980; SPWLA-1980-P. OnePetro: Richardson, TA, USA, 1980.
40. Martin, J.P.; Nicoletis, S.; Raiga-Clemenceau, J. The concept of acoustic formation factor for more accurate porosity determination from sonic transit time data. *Log Anal.* **1988**, *29*, SPWIA-1988-v29n1a4.
41. Gao, J.; Ma, B.; Lu, Y.; Zhang, W.; Cao, Q. Origin of authigenic kaolinite with implications for Permian tight gas sandstone reservoirs in the northern Ordos Basin, central China. *J. Nat. Gas Sci. Eng.* **2022**, *99*, 104429. [[CrossRef](#)]
42. Wang, G.; Chang, X.; Yin, W.; Li, Y.; Song, T. Impact of diagenesis on reservoir quality and heterogeneity of the Upper Triassic Chang 8 tight oil sandstones in the Zhenjing area, Ordos Basin, China. *Mar. Pet. Geol.* **2017**, *83*, 84–96. [[CrossRef](#)]
43. Zhao, G.P. Characterization of fluid inclusions and timing of gas accumulation in Upper Paleozoic reservoirs of Hangjinqi area, Ordos Basin. *Oil Gas Geol.* **2017**, *38*, 905–912.
44. Archie, G.E. The electrical resistivity log as an aid in determining some reservoir characteristics. *Trans. Am.* **1942**, *146*, 41–56. [[CrossRef](#)]
45. Liu, Y.; Ye, J.; Zong, J.; Wang, D.; Cao, Q.; Yang, B.; Li, W.; Zhao, J. Analysis of forces during tight oil charging and implications for the oiliness of the tight reservoir: A case study of the third member of the Palaeogene Shahejie Formation, Qibei slope, Qikou sag. *Mar. Pet. Geol.* **2022**, *144*, 105819. [[CrossRef](#)]
46. He, Y.; Guo, H.; Lan, H.; Ling, C.; Fu, M. The Effect of Single Sandstone Stacking Pattern on the Sandstone Reservoir Physical Properties—A Case Study from the Shanxi Formation in the Daniudi Area, Northeastern Ordos Basin. *Energies* **2022**, *15*, 4740. [[CrossRef](#)]
47. Zhao, G.; Li, X.; Liu, M.; Dong, C.; Chen, D.; Zhang, J. Reservoir Characteristics of Tight Sandstone and Sweet Spot Prediction of Dibeig Gas Field in Eastern Kuqa Depression, Northwest China. *Energies* **2022**, *15*, 3135. [[CrossRef](#)]
48. Wang, R.; Sun, W. A Study on Micro Cracks in Super Low Permeability Sandstone Reservoir of the Upper Triassic Yanchang Formation in the Ordos Basin. *Geol. Rev.* **2009**, *55*, 444–448.

Disclaimer/Publisher’s Note: The statements, opinions and data contained in all publications are solely those of the individual author(s) and contributor(s) and not of MDPI and/or the editor(s). MDPI and/or the editor(s) disclaim responsibility for any injury to people or property resulting from any ideas, methods, instructions or products referred to in the content.